Made available through Montana State University's ScholarWorks

Theoretical and Experimental Insights into CO2 Capture and Methanation over Amine-Grafted Ru-Based Catalysts

Shyam Deo, Thomas Ludwig, Melinda L. Jue, Nathan C. Ellebracht, Mathew J. Rasmussen, James M. Crawford, Matthew M. Yung, Sneha A. Akhade, Simon H. Pang

This document is the Accepted Manuscript version of a Published Work that appeared in final form in The Journal of Physical Chemistry C, copyright ©, [include copyright notice from the published article] after peer review and technical editing by the publisher. To access the final edited and published work see [insert ACS Articles on Request author-directed link to Published Work, see ACS Articles on Request]."

Accessibility Disclaimer:

For a more accessible version of this document, please submit an accessibility request form through the Montana State University Library website.

THE JOURNAL OF PHYSICAL CHEMISTRY C
A JOURNAL OF THE AMERICAN CHEMICAL SOCIETY

pubs.acs.org/JPCC

Article

Theoretical and Experimental Insights into CO_2 Capture and Methanation over Amine-Grafted Ru-Based Catalysts

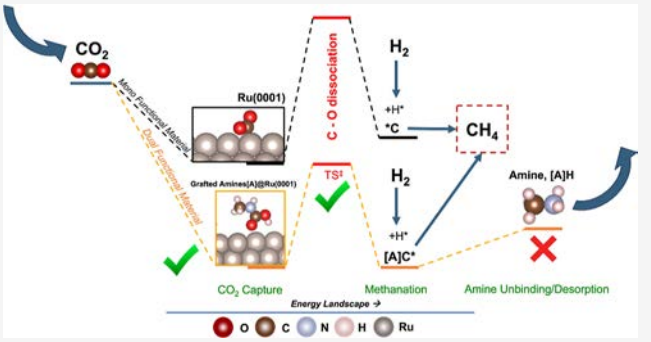
Shyam Deo,*,⊥ Thomas Ludwig,⊥ Melinda L. Jue, Nathan C. Ellebracht, Mathew J. Rasmussen, James M. Crawford, Matthew M. Yung, Sneha A. Akhade,* and Simon H. Pang

Cite This: https://doi.org/10.1021/acs.jpcc.4c08009

Read Online

ACCESS | Metrics & More | Article Recommendations | Supporting Information

ABSTRACT: Carbon capture and storage (CCS) technologies, along with CO_2 capture and conversion methods, have emerged as crucial research areas to address rising CO_2 emissions. In this study, we seek to understand the mechanistic role of amines in enabling lower-energy pathways for CO_2 conversion. Our research focuses on the development and analysis of dual-functional materials (DFMs) engineered for the reactive capture and conversion (RCC) of CO_2 into methane, utilizing Ru catalysts grafted with amine groups. We employ Density Functional Theory (DFT) calculations using methylamine as a model amine to investigate the impact of amine groups on CO_2 methanation on a Ru(0001) surface, both in the presence and absence of amine groups. The amine ligand alters the carbon coordination environment, promoting direct C−O dissociation and potentially destabilizing the CO* adsorbate, thereby reducing the risk of CO poisoning. Additionally, we observe a preference for hydrogenation, although it becomes more energetically uphill in the amine-bound scenario. Our experiments, however, report similar CO_2 conversion and CH_4 production rates over the synthesized catalysts "Ru/TiO_2" and the amine (*N*-(2-aminoethyl)-3-aminoproplytrimethoxysilane ("diaminosilane")) deposited catalyst "diamine-Ru/TiO_2". By constructing comparative reaction-free energy diagrams and performing microkinetic modeling (MKM) simulations, we link our theoretical findings with experimentally observed CO_2 uptake, conversion, and methane production rates. A microkinetic model (MKM) was employed to investigate the anomaly, showing reduced amine−carbon complex coverage and increased CO_2 coverage at all temperatures. The MKM simulations consistently confirmed these trends. This comprehensive approach offers key insights into the role of the amine-CO_2 bond in methanation, highlighting a pathway toward lower-energy, more efficient CO_2 capture and conversion processes.



1. INTRODUCTION

CO_2 emissions play a crucial role in driving global warming and climate change. This phenomenon leads to shifts in weather patterns worldwide, causing alterations in precipitation, more frequent and intense storms, and changes in climate zones. These effects can have severe implications for agriculture, water resources, and ecosystems. Consequently, reducing CO_2 emissions has become a primary objective in the global fight against climate change. Among various initiatives aimed at mitigating these emissions, there is a strong emphasis on promoting carbon capture and storage technologies.[1,2] Moreover, significant advances have been made in converting CO_2 into useful chemicals via methanation/RWGS (reverse water gas shift) reactions.[3,4] However, the low concentration (~400 ppm) of CO_2 in the air necessitates large reactor beds which operate at low temperatures.[5−7] The kinetics for converting CO_2 into useful products, therefore, are very slow, even with catalysts.[7,8] Consequently, a simultaneous advancement of technology for capturing and converting carbon has attracted significant attention[9,10] for higher process efficiency via streamlined operations,[11−14] reduced capital costs and energy savings.[15] The pursuit of materials and technologies that can achieve these dual goals (reactive capture and conversion, RCC) has become a distinct research focus.[16,17]

A potential solution toward RCC lies in the design of dual-functional materials (DFM),[17] which can facilitate the capture of CO_2 from flue gas followed by a methanation process. Several experimental efforts have been made to design DFM materials for combined CO_2 capture and utilization. DFM materials have been designed using a combination of alkali oxides and reactive metal materials to study RCC from point sources. Alkali oxides are effective adsorbents at higher

Received: November 27, 2024
Revised: March 25, 2025
Accepted: March 31, 2025

ACS Publications © XXXX American Chemical Society

temperatures and higher partial pressures of CO_2. For example, Sun et al.[18] synthesized Ce-modified CaO sorbents which exhibited outstanding CO yield from the dissociated CO_2 over the oxygen vacancies of the ceria support. Moreover, Arellano-Trevino et al.[19] reported alkaline (Na_2O) adsorbent with methanation catalysts (Ru, Pt, and Pd) supported on γ-Al_2O_3. When moving from a point source (e.g., ∼4−20% CO_2) capture to air capture (0.04%),[5−7] it would be sensible to consider capture chemistries that have been proven to be more favorable for CO_2 capture from air. In this regard, amines are a state-of-the-art material class for CO_2 capture from air and have rapid capture rates and high capacities.[20,21] The metal catalyst particles can then catalyze the conversion of the captured CO_2 to methane.[22] For example, Crawford et al.[23] demonstrated low-temperature activation of H_2 and increased activation of CO_2 over Ru/TiO_2 catalysts. Since catalytic methanation over metallic surfaces is well-studied and known[7,24] there is a potential for synergy between the capture and the conversion steps when using amines. Consequently, we hypothesize that an amine-bound CO_2 may access alternative, lower-energy conversion pathways. However, the interactions between the capture and catalysis processes is still not well understood. For example, the chemically captured CO_2 can directly react to form methane while still being bound to the amine ligand. Alternatively, it can first unbind from the amine and then react as pure CO_2, following a conventional CO_2 methanation heterogeneous catalysis mechanism.[22] A comprehensive analysis using theory and experiment collaboration is required where the two processes can be selectively isolated for experimental study, and Density Functional Theory (DFT)[25] can provide mechanistic insights for the experimental observations. Such integration is practically significant for accurately estimating the cost-based performance of DFMs since it critically relies on an amine-catalyst synergy over the course of the reaction mechanism. This paper aims to study this potential synergy for alternative amine-based DFM materials.

In the current study, we employed DFT calculations to study the impact of the amine ligands on the CO_2 methanation reaction, which offers a promising avenue to gain valuable insights into the underlying reaction mechanisms and the role of the amine group in influencing the reaction energetics. Our investigation involved developing appropriate molecular models for the reactants, intermediates, and products during amine-assisted (amine-bound) and conventional pathway (nonamine-bound) toward CO_2 methanation on Ru(0001) surface. The use of the Ru system is intended to qualitatively examine the reactive carbon capture process on our experimentally synthesized Ru/TiO_2 catalyst and the Diamine−Ru/TiO_2 catalyst (Ru grafted with amines). Experimentally, CO_2 conversion and methanation rates are contrasted across the "Ru/TiO_2" and the "Diamine−Ru/TiO_2" catalysts. Through our theoretical and experimental study, we explored various reaction pathways and intermediate species, with a primary focus on comparing the reaction mechanisms between the two mentioned pathways. Specifically, we investigated how the presence of the amine group might act as a catalyst or provide additional active sites, thereby affecting the overall energetics of the reaction. To analyze and interpret the results, we constructed comparative reaction-free energy diagrams, allowing us to qualitatively interpret any shifts in the favorable reaction mechanisms and identify likely rate-determining steps. Toward the end, microkinetic modeling (MKM) simulations were also used to interpret the gaps between the simulated and experimentally observed product selectivity, CO_2 conversion, and methane production rates. This comprehensive approach will enhance our understanding of the role of the amine-carbon bond in the CO_2 methanation reaction and provide valuable insights for potential applications in carbon capture and utilization processes.

2. METHODS

2.1. Electronic Structure Methods. All Density Functional Theory (DFT) calculations were performed using the Vienna ab initio Simulation Package (VASP) version 5.4.4[26−28] within the atomic simulation environment (ASE).[29] The electron exchange and correlation energies were computed using the Revised Perdew, Burke, and Ernzerhof (RPBE)[30] version of the generalized gradient approximation (GGA) functional. The projector-augmented wave (PAW) method was employed to describe the ion−core electron interactions with a kinetic energy cutoff of 400 eV for surface calculations.[31,32] Geometries were optimized with a force convergence criterion of 0.02 eV/Å and total energies were converged to at least 10^{-5} eV. A Methfessel-Paxton smearing of 0.10 eV was used for all the calculations.[33] All bulk, surface, and gas phase calculations use a nonspin polarized methodology. Vibrational energy calculations were performed in VASP, and the thermochemistry module within the Atomic Simulation Environment (ASE) package.[29] Zero-point vibration energies (ZPVE) and free energy (ΔG) corrections for both adsorbates and gas-phase species were computed using the harmonic and ideal gas approximations unless otherwise mentioned. Total energies of the molecules in the gas phase were calculated using spin polarization in a 15 Å × 15 Å × 15 Å unit cell with 1 × 1 × 1 k-point mesh.

2.2. Surface Model. To examine the impact of the amine ligand on the energetics of CO_2 methanation catalysis, we established a simplified model of the amine ligand for use in the catalysis simulations. We validated this by comparing the reaction energies of this simplified model to those of more complete models (Supporting Information Note S1). In particular, we found that among the various amine structure models (Figure S1), using methylamine as the model amine ligand resulted in very similar reaction energies (within 0.1 eV for carbamic acid formation, an essential amine−surface binding step as detailed later in section Amine Binding) to those using the full aminopropylsilane ligand (Figure S3). The reaction schematic is shown in Supporting Information Note S1, Figure S2. The similarity led us to select the methylamine model as a suitable compromise between model complexity and, computational cost and accuracy for the catalysis calculations. While the full aminopropylsilane structure may be important in modeling other aspects of the system, such as the effect of the support on the grafted polymer dynamics[34] or the effect of the polymer degrees of freedom[35] on the CO_2 capture, we can confidently assert that the simplified model accurately captures the primary chemical reaction energy effects driving the surface catalytic conversion. Furthermore, given the experimental uncertainty regarding the kinematics and dynamics of unadsorbed grafted amine states [A]H[36] and the absence of a standardized model for the entropy of a free end of a grafted polymer,[37,38] we opted to model the unadsorbed grafted amine states as gas-phase states. This is one of two limiting cases for modeling the entropy of the

https://doi.org/10.1021/acs.jpcc.4c08009
J. Phys. Chem. C XXXX, XXX, XXX−XXX

unadsorbed, grafted amine states in this work; the other would be to neglect all translational and rotational entropy, in which case the entropy would be identical to that of an adsorbed state. In reality, due to the translational and rotational degrees of freedom available to the unadsorbed surface-grafted polymer states, the entropy of such states is likely to be meaningfully greater than that of a surface adsorbate, but less than that of a gas phase state. We acknowledge that the choice of entropy model for the unadsorbed grafted amine states $[A]C_xO_yH_z$ would influence the reaction entropy and, consequently, the free energies of adsorption and desorption elementary steps involving the amine state. This approach captures the increased translational and rotational entropy of these states compared to chemisorbed surface species due to the mobility of the bound polymers, though it is likely an overestimate. Thus, the gas-phase-limit model for the entropy would result in a greater entropic penalty for adsorption of these states, and is likely to overpenalize the real adsorption energy (due to the entropic adsorption penalty) and thus underpredict the coverages. If one instead chooses to neglect the translational and rotational entropies of these states, the coverages would likewise be overpredicted. The reality is somewhere in between the gas-phase and adsorbate limits, and this is a point that would benefit from dedicated future work. Finally, we note that due to the nature of reaction network kinetics, this choice of entropy model is only expected to affect the rate results if an adsorption or desorption step of these surface-grafted amine states is found to be rate-limiting. If not, then the choice of entropy model could still affect the surface coverages, but would be unlikely to affect any rate results or rate trends. The implications over the CO_2−amine binding are further discussed in Section Initial Adsorption.

As a first approach to modeling the Ru catalyst particles, we used a (3 × 3) 3-layered Ru surface slab (0001) (Figure S4). Even if the particles are relatively small, the surface slab should be a useful approximation for the primary goal of determining the effect of the amine ligand on the methanation mechanism. A close-packed Ru(0001) has been a common model for the conventional (nonamine-bound) CO_2 methanation reaction in previous works,[39] as it represents a dominant and relatively stable facet on Ru nanoparticles. The atomic positions on the bottom two layers were frozen at their bulk lattice positions during structural optimizations. In all surface calculations, a vacuum distance of at least 12 Å was used between the repeating slab images, and dipole corrections[40] were applied to cancel spurious interactions between the periodic images. A Γ centered *k*-point mesh of 4 × 4 × 1 was used with the third vector perpendicular to the surface for calculations on the surface unit cells.

Reaction energies were determined as the energy difference between the initial and final states of an elementary reaction. Transition states (TS) were located using the climbing image nudged elastic band (CI-NEB) method[41](5−7 images) by relaxing the force below 0.05 eV/Å. The TS state was confirmed by the presence of a single imaginary frequency along the reaction coordinate. Activation energies for reactions were then calculated as the energy difference between the initial and transition states of the elementary reaction.

2.3. Experimental Details. *2.3.1. Catalyst Synthesis and Characterization.* Catalysts were prepared via strong electrostatic adsorption (SEA) of a $Ru(NH_3)_6Cl_3$ precursor (hexaaminеruthenium(III) chloride, Sigma-Aldrich, 99.9% trace metal basis) on TiO_2 microspheres (500 μm diameter, Johnson Matthey). Aqueous ammonia (56.6 wt %, Sigma-Aldrich, ACS reagent) was used to adjust the pH of DI water (>14 M Ωcm) to pH = 9. The TiO_2 support was dispersed in a beaker of pH 9 DI water, while the Ru precursor was dissolved in a second beaker of water (5 wt % Ru loading in the final sample). Each solution was allowed to equilibrate for 30 min prior to gradual introduction of the Ru solution through a buret to the TiO_2 suspension under stirring. The combined solution was mixed on a shaker plate at 150 rpm for 24 h. The Ru loaded TiO_2 spheres were then removed from the liquid, dried overnight at 110 °C, and washed with 500 mL/g of 0.1 M NH_4OH solution to remove chlorine impurities. Finally, the catalysts were calcined in air, heating to 300 °C for 3 h with a ramp rate of 10 °C/min in a muffle furnace. This sample is referred to as "Ru/TiO_2" in this work. For more information, readers are encouraged to refer to the paper.[42]

An aliquot of the Ru/TiO_2 sample was reserved for amine deposition. Due to the high temperature calcination required for Ru deposition, the amine deposition was performed after the Ru to avoid amine degradation. The 5Ru/TiO_2 was dried overnight under vacuum at 100 °C in Erlenmeyer flasks prior to grafting. Flasks were backfilled with Ar and transferred to a shaker plate (100 rpm) and 25 mL of toluene per g support was added via syringe. Samples were agitated for at least 30 min before 0.2 g DI H_2O per g support was added via syringe and allowed to equilibrate for an hour. Next, 3 mmol of *N*-(2-aminoethyl)-3-aminoproplytrimethoxysilane ("diaminosilane") per g support, dispersed in 1−2 mL of toluene, was introduced dropwise via syringe. The mixture was agitated (100 rpm) overnight at room temperature (~22 °C). The grafting solution was decanted from the solids and then the spheres were rinsed with 100 mL per g each of methanol, toluene, hexane, and methanol again in a vacuum filter before drying at 80 °C in a vacuum oven. This sample is referred to as "Diamine-Ru/TiO_2" in this work. For additional details, readers should consult the paper.[42] Furthermore, the pattern of amine grafting on Ru/TiO_2 and its characterization are thoroughly detailed in our published perspective[42] and summarized in the Supporting Information Note S3. Essentially, a significant concentration of amines is expected near the Ru, as the aminosilanes are grafted onto both the titania and each other. While it is possible that oligomeric silanes may partially cover some Ru nanoparticles on the surface or that certain amines could coordinate with the metal sites, these possibilities remain unconfirmed by direct evidence.

2.3.2. Reactor Setup Conditions. Steady-state methanation experiments were performed in a Micromeritics Microactivity Effi Reactor connected to a downstream mass spectrometer (UGA HT200 Universal Gas Analyzer, SRS). For each experiment, ~75 mg of catalyst was loaded into a stainless-steel fritted reactor tube and reduced in situ under 100 sccm H_2 while heating at 200 °C (10 °C/min ramp rate) for 1 h. Samples were then cooled under H_2 to 110 °C prior to reaction. Steady state catalytic activity measurements were taken in 10 °C increments from 110 to 200 °C in an atmosphere consisting of 2 sccm H_2 and 3 sccm 10% CO_2/ balance He. A 6.67:1 H_2/CO_2 molar ratio was chosen to provide an excess of H_2, compared to the stoichiometric 4:1 molar ratio. The reaction pressure was held at ambient pressure in Golden, CO (~0.85 bar). At each reaction temperature, the catalyst bed was exposed to the reactive gases for 60 min to allow for a steady state to occur. The methane production rates were calculated based on the m/z =

https://doi.org/10.1021/acs.jpcc.4c08009
J. Phys. Chem. C XXXX, XXX, XXX−XXX

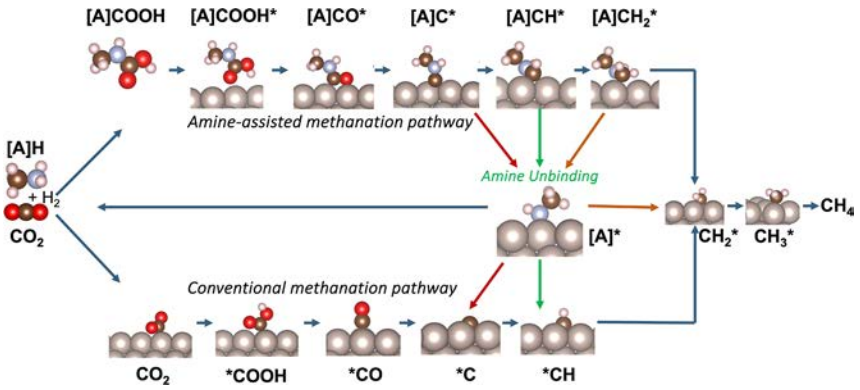


Figure 1. Proposed reaction mechanism for amine-assisted (amine-bound; top) and conventional pathway (nonamine-bound; bottom) toward CO_2 methanation on Ru(0001) surface. [A]H refers to the gas phase methylamine(CH_3NH_2). The methylamine in the figure (and in our DFT model) is a computational model that approximates the local chemical environment/bonding of the full surface-bound/grafted amine species on the Ru catalyst surface. Both pathways converge toward different modes of amine unbinding (indicated by distinct arrow colors representing the reactants, intermediates, and products formed through these modes), as observed at the end of the mechanism. Color labels for the atoms are as follows: oxygen (red), hydrogen (light pink), carbon (russet), nitrogen (light blue), and ruthenium (light brown).

15 signal by averaging 100 s of mass spectrometer data near the end of the 60 min reaction step. Conversion of CO_2 was calculated based on the amount of CH_4 produced during the reaction at a given temperature divided by the amount of CO_2 fed to the reactor according to the following eq 1.

$$\text{CO}_2\ \text{Conversion}\ (\%) = \frac{\text{CH}_4\ \text{molar flow rate detected}\ (m/z = 15)\ \text{during reaction}}{\text{CO}_2\ \text{molar flow rate feeding reactor}} \quad (1)$$

Readers seeking more in-depth information can refer to the paper.[42]

3. RESULTS AND DISCUSSIONS

3.1. Mechanistic Determination. Research on the amine-bound CO_2 methanation mechanism over heterogeneous catalysts is still in its early stages, with most studies to date focusing on homogeneous catalysis.[43−45] It is in principle more complex than the conventional CO_2 methanation mechanism because it involves the additional degree of freedom associated with the amine ligands. The amine ligand is in principle capable of binding and unbinding to the carbon species at any stage in the mechanism. Additionally, amines could potentially alter the course of the reaction pathway by assisting a few key elementary steps over a metallic surface. For example, the amines could interact with CO_2 and assist in its activation and reduction, leading to the formation of an intermediate species. This interaction might involve the amine acting as a Lewis base, donating electron pairs to stabilize the CO_2 molecule, or activating it for further reactions. Also, in the presence of hydrogen, the amine ligand [A] may be hydrogenated to form [A]H which can then act as a hydrogen carrier, participating in hydrogenation steps during the reaction. Therefore, here we studied and compared the CO_2 methanation mechanism between the amine-assisted (amine-bound) and the conventional (nonamine-bound) pathways. In our discussions, gas-phase methylamine (CH_3NH_2) is noted as [A]H, so [A] refers to the methylamine missing one hydrogen, or the amine ligand. We do this because [A], the amine ligand, is what directly coordinates with the various carbon (C) species (and, potentially, with the surface as [A]* where * denotes bonding to the catalyst active site).

In CO_2 methanation, various elementary steps are involved, as schematically shown in Figure 1. The figure highlights the correlation between amine-bound and nonamine-bound routes, although not exhaustively displaying all intermediates and reaction energies calculated. The reactants (CO_2 and H_2) are transformed into products (CH_4 and H_2O) through a sequence of elementary steps. Typically, a conventional methanation pathway (nonamine bound) (Figure 1) involves the dissociation of both C−O bonds (of CO_2) and a total of eight hydrogenation steps (two hydrogenations for each oxygen atom to form H_2O and four hydrogenations for carbon to form CH_4), apart from the adsorption and desorption steps.[22] The actual mechanism depends on the relative ordering of C−O dissociation and hydrogenation steps (for both C and O). This sequence determines the dominant intermediates observed along the pathway and the reaction energies and barriers constituting the overall mechanism. Numerous studies have investigated this aspect in the context of conventional methanation reactions.[22] For example, Yu et al.[22] showcased differences in mechanism from the onset of CHO* generation, where Ru/$RuTiO_2$ favors further hydrogenation toward CH_2O* (an associative mechanism). In contrast, Ru/TiO_2 favors direct C−O bond cleavage in a dissociative fashion. Additionally, in the conventional pathway, H_2 undergoes dissociative adsorption on the catalyst as H*, facilitating hydrogenation of the generated carbonaceous radicals. The influence of an amine on the methanation pathway includes amine and CO_2 binding as carbamic acid or ammonium-carbamate ion pairs,[35,46] followed by initial dissociative adsorption of CO_2, CO dissociation, successive hydrogenations (all occurring while amine is attached to the C* moiety), and eventual amine unbinding (Figure 1). The amine-bound and conventional pathways would merge after the CH_2* state due to carbon's valency of four, which prevents simultaneous binding to the surface and four other atoms (H, H, H, N). The precise step where the amine ligand detaches remains undetermined and could potentially occur prior to the [A]CH_2* state ([A] stands for a gas phase methylamine ligand (CH_3NH−)). As a result, the presence of an amine can modify the energetics and surface affinity of specific reaction intermediates due to their attachment to an amine site, potentially leading to a lower-energy pathway, which will be explored in the following section.

https://doi.org/10.1021/acs.jpcc.4c08009
J. Phys. Chem. C XXXX, XXX, XXX−XXX

Table 1. List of Elementary Steps and Their Reaction Energetics (ΔE_{rxn}) for CO_2 Methanation Reaction via the Amine-Assisted Pathway (Amine-Bound) over the Ru(0001) Surface as Shown in Figure 6[a]

index	elementary Steps	ΔE_{rxn} (E_a), eV
0	CO_2 + [A]H + 4H_2 ↔ CO_2 + [A]H + 8H*	−0.68
1	CO_2 + [A]H + 8H* ↔ [A]COOH + 8H*	0.87
2	[A]COOH + 8H* ↔ [A]COOH* + 8H*	0.40
3	[A]COOH* + 8H* ↔ [A]CO* + OH* + 8H*	−0.12
4	[A]CO* + OH* + 8H* ↔ [A]CO* + H_2O + 7H*	−0.27
5	[A]CO* + H_2O + 7H* ↔ [A]C* + O* + H_2O + 7H*	−0.13 (1.53)
6	[A]C* + O* + H_2O + 7H* ↔ [A]C* + OH* + H_2O + 6H*	0.34
7	[A]C* + OH* + H_2O + 6H* ↔ [A]C* + 2H_2O + 5H*	−0.27
8	[A]C* + 2H_2O + 5H* ↔ [A]CH* + 2H_2O + 4H*	0.48 (0.68)
9	[A]CH* + 2H_2O + 4H* ↔ [A]CH_2* + 2H_2O + 3H*	0.32
10	[A]CH_2* + 2H_2O + 3H* ↔ [A]H + CH_2* + 2H_2O + 2H*	−0.43
11	CH_2* + 2H_2O + 2H* ↔ CH_3* + 2H_2O + H*	0.06
12	CH_3* + 2H_2O + H* ↔ CH_4 + 2H_2O	−0.96

[a]The parentheses list the activation energy (E_a) for the corresponding steps. [A]H and [A]COOH refer to the gas phase methylamine and the gaseous carbamic acid respectively. The free energies tabulated are DFT-calculated free energies (in eV) at 450 K.

Based on DFT calculations using methylamine as the model amine (Supporting Information Note S1), we proposed a set of elementary reaction steps constituting the catalytic conversion of amine-bound CO_2, in correspondence with previously studied and established nonamine-bound mechanisms. From these proposed steps, we identified all distinct adsorbed intermediates. We then set up models of all these intermediates and proceeded to calculate their energies using DFT calculations, using the harmonic approximation to calculate free energy corrections (zero-point energy, heat capacity, and entropy corrections) at 300, 450, and 600 K to encompass the steady−state reaction temperatures. From these total energies, we calculate the binding energies, which are essentially formation energies, such that reaction energies for any possible elementary step involving the included intermediates can be readily calculated. Using this approach allows us to study a variety of resulting pathways, without having to calculate each reaction energy explicitly any time a new elementary step is to be included, unless that step involves an adsorbate not previously considered.

The reaction energies and the activation barriers (for certain steps) are tabulated in Tables 1 and 2 for the amine-assisted and the conventional amine-free pathway, respectively. The exact kinetics of certain elementary steps like H_2O formation from H* and OH*, second hydrogenation, etc. among others, have not been considered and we refer the reader to existing published studies that report kinetic information.[47−49] The following sections explore the entire mechanism step by step, beginning with amine binding, followed by initial CO_2 species adsorption, CO dissociation, full hydrogenation, and finally, amine unbinding. A comparison and discussion of the reaction free energy diagrams are presented, illustrating the mechanistic pathway of CO_2 methanation reaction for both the amine-bound and the nonamine-bound routes. We then discuss the experimental CO_2 conversion and the methane production rates over the "Ru/TiO_2" and the "Diamine-Ru/TiO_2" catalysts. Toward the end, microkinetic modeling (MKM) simulations are also discussed to interpret the gaps between the simulated and experimentally observed product selectivity, CO_2 conversion, and methane production rates.

3.1.1. Amine Binding. When CO_2 reacts with an amine such as the aminopropylsilane ligand, it can predominantly form a carbamate ion species (likely in association with a cation such as an ammonium species, forming an ammonium-carbamate ion pair).[35,46] This ammonium-carbamate ion pair exists in chemical equilibrium with a carbamic acid species (in the fashion carbamic acid + amine ↔ ammonium carbamate, or simply, $RNHCOOH + RNH_2 \leftrightarrow RNHCOO^- + RNH_3^+$, assuming primary amines) with nearly identical free energies and a low free energy barrier for proton transfer.[50] The only distinction between ammonium carbamate and carbamic acid lies in which species is protonated-the adjacent spectator amine or the CO_2 group bound to the amine.[35] Due to the complexities of modeling reactions involving ionic species in DFT, we primarily consider carbamic acid ([A]COOH) formation (hereafter also termed interchangeably as "amine−carbon complex", AC). We note that the choice of ammonium-carbamate ion pair vs carbamic acid would only affect a single step in the catalytic mechanism (the adsorption step) and that all other steps are unaffected by this choice since their reaction

Table 2. List of Elementary Steps and Their Reaction Energetics (ΔE_{rxn}) for CO_2 Methanation Reaction via the Conventional Pathway (Non-Amine-Bound) over the Ru(0001) Surface as Shown in Figure 6[a]

index	elementary Steps	ΔE_{rxn} (E_a), eV
0	CO_2 + 4H_2 ↔ CO_2 + 8H*	−0.68
1	CO_2 + 8H* ↔ CO_2*+ 8H*	1.17
2	CO_2* + 8H* ↔ COOH* + 7H*	−0.06
3	COOH* + 7H* ↔ CO* + OH* + 7H*	−0.71
4	CO* + OH* + 7H* ↔ CO* + H_2O + 6H*	−0.27
5	CO* + H_2O + 6H* ↔ C* + O* + H_2O + 6H*	0.81 (2.67)
6	C* + O* + H_2O + 6H* ↔ C* + OH* + H_2O + 5H*	0.34
7	C* + OH* + H_2O + 5H* ↔ C* + 2H_2O + 4H*	−0.27
8	C* + 2H_2O + 4H* ↔ CH* + 2H_2O + 3H*	−0.18 (0.66)
9	CH* + 2H_2O + 3H* ↔ CH_2* + 2H_2O + 2H*	0.36
11	CH_2* + 2H_2O + 2H* ↔ CH_3* + 2H_2O + H*	0.06
12	CH_3* + 2H_2O + H* ↔ CH_4 + 2H_2O	−0.96

[a]The parentheses list the activation energy (E_a) for the corresponding steps. The free energies tabulated are DFT-calculated free energies (in eV) at 450 K. Note: the reaction index 10 from the Table 1 corresponds to the amine unbinding energetics which is inapplicable for the conventional amine-free pathway and therefore excluded.

https://doi.org/10.1021/acs.jpcc.4c08009
J. Phys. Chem. C XXXX, XXX, XXX−XXX

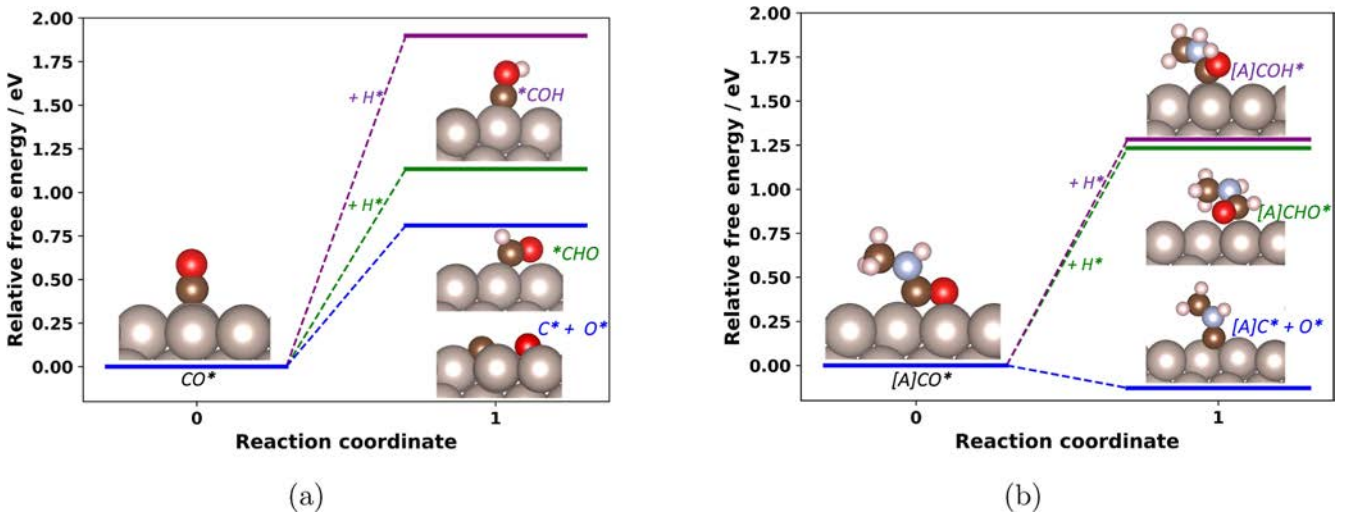


Figure 2. Thermodynamic free energy diagrams for C−O dissociation, CO hydrogenation to COH, and CHO via (a) a conventional pathway (nonamine-bound: CO* ↔ C* + O*, CO* + H* ↔ COH*, and CO* + H* ↔ CHO*, respectively) over the Ru(0001) surface and (b) that via an amine-assisted pathway (amine-bound: [A]CO* ↔ [A]C* + O*, [A]CO* + H* ↔ [A]COH*, and CO* + H* ↔ [A]CHO*, respectively), showcasing the effects of amine ligands on the C−O dissociation and hydrogenation. [A] refers to the methylamine missing one hydrogen, or the methylamine ligand (CH_3NH-). The free energies shown are DFT-calculated free energies (in eV) at 450 K.

energies and barriers do not involve this species (see Supporting Information Note S5, Carbamic Acid and Carbamate Equilibrium). Therefore, the results of our study are expected to be robust to this choice unless the rate-determining step is the initial adsorption step, which is not hypothesized to be the case in either the conventional[39,49] or the amine-bound CO_2 methanation mechanism.[9] The question of the equilibrium between ammonium-carbamate and carbamic acid, and the degree to which this equilibrium is affected by the presence of either the oxide support or the nearby Ru catalyst particles, as well as the density of grafted amines and the reaction conditions (for example, the activity of H_2O near the surface), could be an interesting area of study for future work. The schematic for carbamic acid formation via methylamine and other amine structures is shown in Section Supporting Information Note S1, along with their reaction energies. As discussed earlier, in Section 2.2, using methylamine suffices for the purpose of modeling amine interaction with CO_2 and the corresponding energetics toward the CO_2 methanation.

3.1.2. Initial Adsorption and Reaction of CO_2 Species. The adsorption of CO_2 is quite weak on the Ru(0001) surface in both the amine-bound and the conventional case. This indicates that dissociative adsorption after hydrogenation (CO* and OH*) is likely a realistic assumption.[39] The ammonium-carbamic acid adsorption as [A]COOH* and the adsorption of CO_2 as COOH* are shown in Figure 1. The corresponding binding energies are −0.26 and 0.32 eV, respectively. Thereafter, the dissociative adsorption (as CO*) is shown in Figure 2a,b for the conventional and the amine-bound pathways, respectively. The reaction energies for the dissociative adsorption are −0.16 eV (amine) vs −0.69 eV (nonamine). The enthalpic difference is primarily due to the additional stabilization of the departing species CO* by the amine group. Furthermore, the choice of entropy model using the unadsorbed grafted amine states does not impact the entropy change of this carbon capture elementary step. In this reaction, the entropy change is given by $\Delta S = S([A]COOH) - S(CO_2) - S([A]H)$, where the entropy term (S) for the [A] state appears on both sides, ensuring that the net loss of one gas-phase entropy unit from the CO_2(g) state remains unchanged. Future work could explore a more refined treatment of the entropy of desorbed grafted amine states to enhance modeling accuracy for grafted amines.

3.1.3. CO Dissociation. It is likely that in both the amine-bound and the conventional pathways, the direct dissociative adsorption of CO_2 to CO and O is the first step in the mechanism. CO is a particularly interesting intermediate both because it is itself relatively stable and has even been hypothesized to be poison[51] and because there are multiple possible reactions branching from this intermediate: hydrogenation of either the C or O atom, or direct C−O dissociation.[52] Some studies have found that the direct C−O dissociation has a very high barrier (multiple studies have found this barrier to be in excess of 2 eV[39] although the presence of step sites can lower the barrier relative to a close-packed surface,[53] it may still be prohibitively high) and that the dissociation barrier can be substantially lowered by first hydrogenating the CO species (either to COH or CHO) prior to the C−O dissociation.[39] Therefore, a preponderance of studies[39,52] has suggested that for CO in particular, on metals similar to Ru, at least one hydrogenation step (either to COH or CHO, depending on the catalyst in question) is likely to occur prior to dissociation (Figure 2a).

We find that the amine ligand radically changes this situation. With the amine ligand present, the direct C−O dissociation is thermodynamically much more favorable than the prior hydrogenation of either the C or O (Figure 2b). In fact, the kinetic barrier for [A]C−O dissociation is lowered by more than 1 eV relative to the barrier without the amine present. The result is shown in Figure 3. The final state C* is relatively under-saturated (without the amine) and thus potentially unstable (Figure 2a). Therefore, it results in the amine-bound step being more downhill than more uphill, as in the nonamine case.

3.1.4. C−H Hydrogenation. After C−O dissociation, the carbon radical is exposed to subsequent hydrogenations. The question is whether the amine exerts a similarly strong effect

https://doi.org/10.1021/acs.jpcc.4c08009
J. Phys. Chem. C XXXX, XXX, XXX−XXX

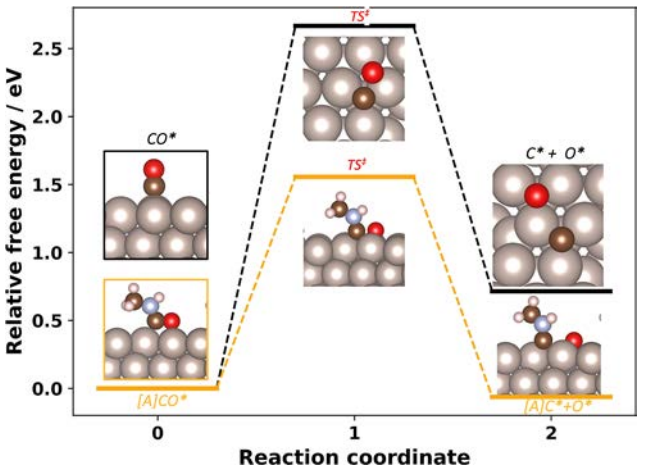


Figure 3. Thermodynamic free energy diagram for C−O dissociation barrier over the conventional pathway (nonamine-bound: -- (black)) and over the amine-assisted pathway (amine-bound: -- (orange)) over the Ru(0001) surface. [A] refers to the methylamine missing one hydrogen, or the methylamine ligand (CH_3NH-). The free energies shown are DFT-calculated energies (in eV) at 450 K.

on hydrogenation, as it does for C−O dissociation. Our calculations of energetics show that the presence of the amine ligand on the carbon atom can stabilize the carbon atom when it is otherwise under-saturated; for example, in the step C* + H* ↔ CH*, the initial state C* is relatively under-saturated, and thus potentially unstable. In the nonamine-bound case, this step is downhill in energy (Figure 4a). But in the amine-bound case, the amine already stabilizes the initial state C*, so the resulting reaction is uphill in energy. However, our results indicate that the first hydrogenation reaction barrier is similar regardless of the presence of the amine (Figure 4b). As for the second hydrogenation, the reaction energy is less uphill in the amine-bound case (0.22 eV vs 0.38 eV in the conventional pathway). This is shown in the second leg of the reaction coordinate in Figure 4a (steps 1−2).

3.1.5. Amine Unbinding. Due to the basic ability of the carbon atom to form at most 4 bonds (just by its valency), the carbon atom is "saturated" as a [A]CH_2* adsorbate, after which the amine must unbind from the carbon atom for further hydrogenations to occur. Therefore, from one perspective, we can compare the amine-bound and the conventional CO_2 methanation pathways up until this point, after which the pathways share the final two hydrogenation steps from CH_2* to methane. In a more rigorous treatment, however, the amine is not constrained to remain bound to the carbon until the last possible step (which is the CH_2* species). Instead, it can, in principle, unbind from the carbon at any stage in the pathway. The various possibilities for amine to unbind are shown in Figure 5. Our calculations show that the amine unbinding is downhill in energy in every step except the unbinding from the [A]C* adsorbate. This is for the same reason as mentioned for the C−O dissociation and the hydrogenation steps. Unbinding from the [A]C* adsorbate results in C* (highly unstable), and hence the uphill energetics (Figure 5b). Unbinding at every other stage always results in a highly coordinated C* (CO*, CH*, or CH_2*) than the above step, and therefore, the energetics are downhill rather than uphill (Figure 5a,c,d). Furthermore, the eventual restoration of the amine ligand after hydrogenation ([A]* + H* ↔ [A]H) is also downhill in energy in all the discussed scenarios.

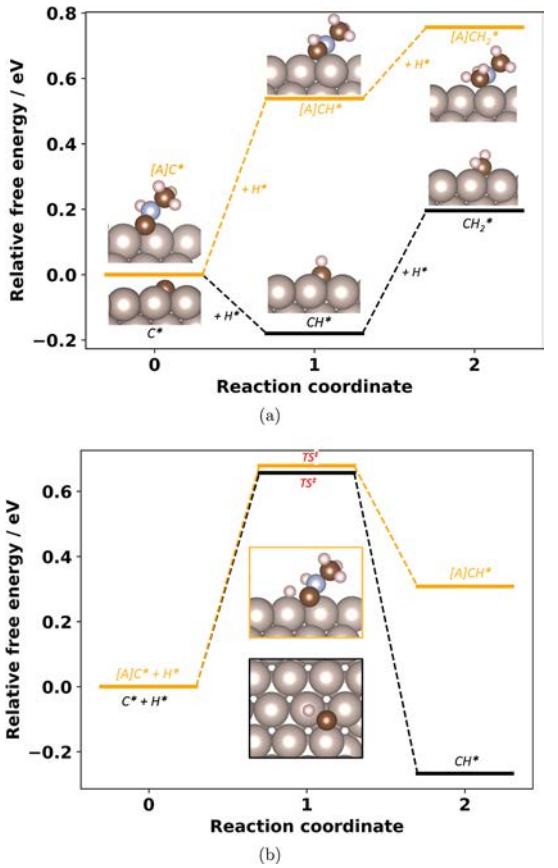


Figure 4. (a) Thermodynamic free energy diagram for carbon hydrogenations (first hydrogenation, [A]C*/C* + H* ↔ [A]CH*/CH* and second hydrogenation, [A]CH*/CH* + H* ↔ [A]CH_2*/CH_2*) over the conventional pathway (nonamine-bound: -- black) and over the amine-assisted pathway (amine-bound: -- (orange)) over the Ru(0001) surface. The free energies shown are DFT-calculated energies (in eV) at 450 K. (b) The thermodynamic free energy barriers for carbon hydrogenation (first hydrogenation, [A]C*/C* + H* ↔ [A]CH*/CH*) over the conventional pathway (nonamine-bound: --) and over the amine-assisted pathway (amine-bound: --) over the Ru(0001) surface. The reactants and the final states are shown in the subplot (a) under the reaction coordinate 0−1. [A] refers to the methylamine missing one hydrogen, or the methylamine ligand (CH_3NH-). The free energies shown are DFT-calculated energies (in eV) at 450 K.

These considerations offer valuable insights into how the amine ligand could potentially influence the energetics of CO_2 methanation. They also present promising avenues for ongoing research, aiming to gain a deeper understanding of these effects. Furthermore, it may be beneficial to calculate the reaction barriers related to the most challenging steps in any feasible mechanisms to facilitate meaningful comparisons. Nevertheless, our calculations of the thermodynamics related to amine stabilization are comprehensive enough to illustrate the supportive role it plays in CO_2 methanation. Additionally, CH_4 methanation generates water, which could protonate amines into ammonium species within the amine-assisted pathway. However, we do not expect this to hinder CO_2 binding in the presence of water. On the contrary, water is well-known to enhance CO_2 capture by amines[54,55] and subsequently facilitate methanation through bicarbonate formation[56] (Supporting Information Note S4).

https://doi.org/10.1021/acs.jpcc.4c08009
J. Phys. Chem. C XXXX, XXX, XXX−XXX

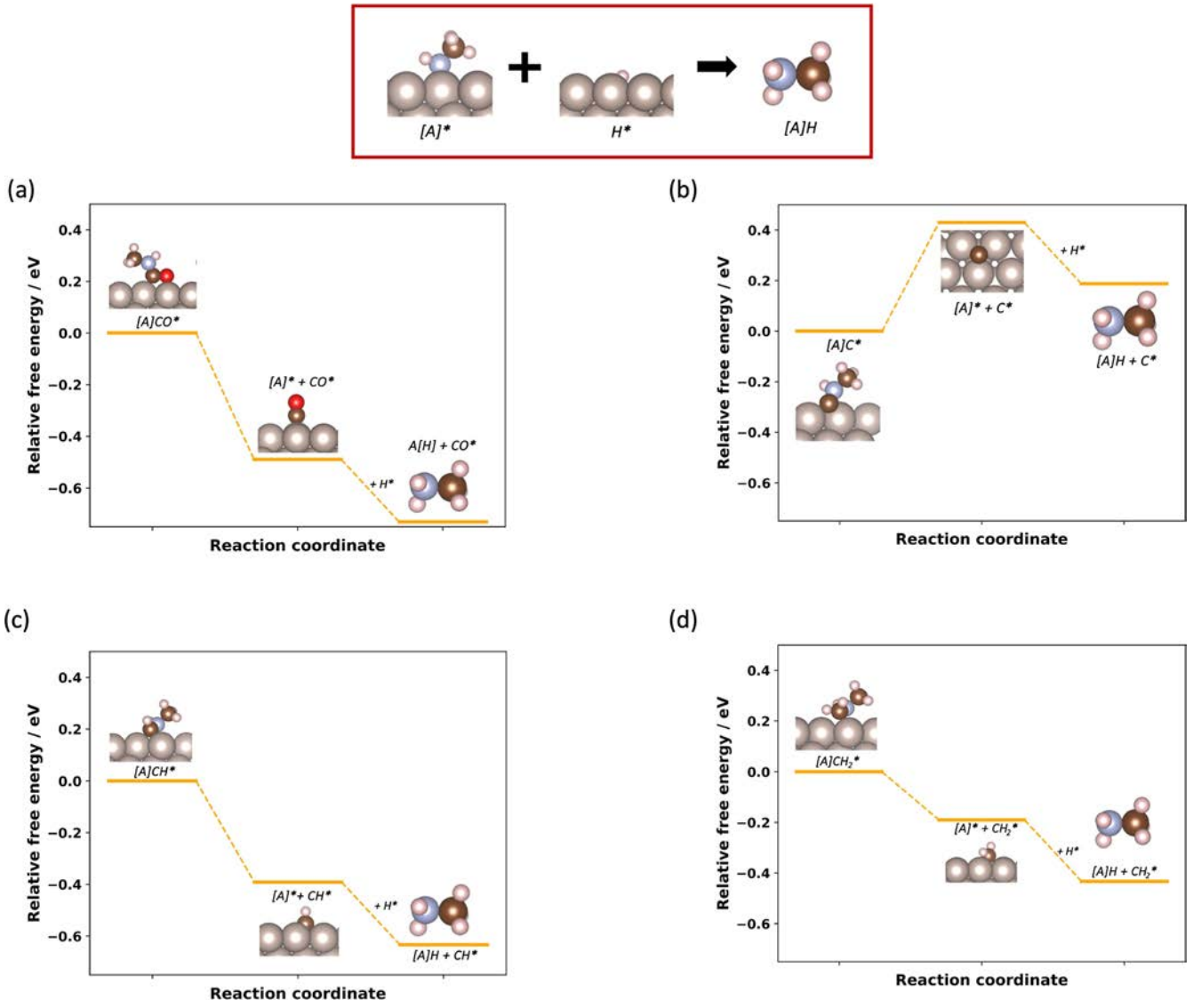


Figure 5. Thermodynamic free energy diagrams of amine unbinding from various amine−bound intermediates—(a) [A]CO*, (b) [A]C*, (c) [A]CH*, and (d) [A]CH_2* via the amine-assisted pathway (amine-bound) over the Ru(0001) surface. [A]* refers to the surface-adsorbed methylamine ligand (CH_3NH−). The first reaction coordinate (0−1) refers to the amine unbinding from the carbon, forming a bond with the surface as [A]* ([A]X* ↔ X* + [A]*, where X can be either CO, C, CH, or CH_2*), and the second reaction coordinate (1−2) as the surface-bound amine ligand [A]* hydrogenation to [A]H ([A]* + H* ↔ [A]H). The schematic for the elementary reaction coordinates (1−2) is shown at the top with their structures. The free energies shown are DFT-calculated energies (in eV) at 450 K.

3.2. Established Energetics for Conversion of Captured CO_2 into CH_4.

After probing the individual elementary steps during CO_2 methanation and establishing the assisted role of amine ligands in stabilizing certain reaction intermediates, it is worthwhile to look at a comparative reaction energy landscape for a comprehensive analysis. Here, the reaction energies and activation barriers, as discussed in the previous sections, are represented in a free energy diagram format for a full mechanistic analysis. To explore how the presence of the amine ligands influences the catalytic pathway, we make a comparison between the amine-bound mechanism and the corresponding nonamine-bound mechanism. As discussed in the previous sections, the thermodynamic and kinetic calculations for all the corresponding intermediates in the absence of the amine ligands, enable us to conduct a similar analysis for the "amine-free" CO_2 methanation reaction.

The results of an initial free energy diagram (at T = 450 K) for a full proposed amine-bound CO_2 methanation pathway over a Ru(0001) surface are shown in Figure 6. A complete list of elementary steps for the mechanism in the figure is presented in Table 1. These elementary steps follow the same order of steps as presented in Figure 1. The overall reaction is $CO_2 + 4H_2 \leftrightarrow 2H_2O + CH_4$, which is the same for both the amine-bound and nonamine-bound pathways; the difference is in the conversion mechanism from the initial to the final states. The free energy diagrams are plotted with reference to the gas phase energies of CO_2 molecules and 8H* adsorbed species, consistent with the overall reaction (Figure 6). The corresponding pathways for the "non-amine bound"CO_2 methanation reaction are also presented in the Figure for comparison. Using these free energy diagrams, one can quickly identify reactions in the mechanism that are highly unfavorable and therefore may not contribute significantly to overall CO_2

https://doi.org/10.1021/acs.jpcc.4c08009
J. Phys. Chem. C XXXX, XXX, XXX−XXX

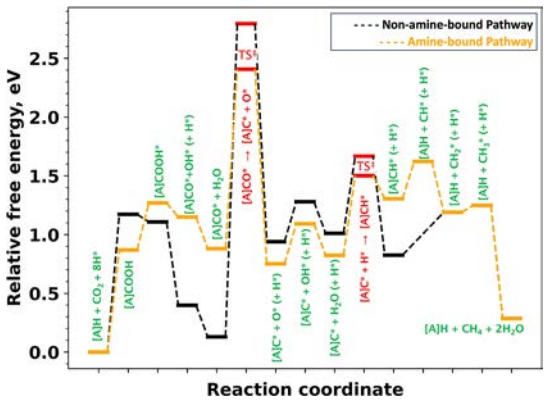


Figure 6. Free energy diagrams for conventional (nonamine-bound: -- (black)) and amine-assisted (amine-bound: -- (orange)) CO_2 methanation reaction pathways on the Ru(0001) surface. The mechanisms are aligned so that the states at the same reaction coordinate are identical up to amine-binding (for example, [A]CO* is aligned with CO*, and [A]CH* is aligned with CH*). [A] refers to the methylamine missing one hydrogen, or the methylamine ligand (CH_3NH-). All energies are reported relative to $CO_2(g)$ + 8H* at a temperature of 450 K and the experimental operating pressure (0.85 bar). The reaction coordinate corresponds to those from the Tables 1 and 2 with the elementary steps noted for the amine-assisted pathway. The H_2 dissociation reactions are therefore excluded from the reaction energy diagram for simplicity (and to reference the four dissociated H_2). $TS^{\ddagger}$ denotes the transition states.

methanation. Additionally, the free energy diagrams at temperatures of 300 and 600 K are shown in Figures S5 and S6, respectively.

As depicted in Figure 6, the only distinction between the amine-bound and the nonamine-bound pathways regards the presence of the amine ligand, denoted as [A]. It is essential to note that differences exist at the beginning and the end of the pathway. Specifically, there are a few steps associated with the CO_2 capture by the amine, as well as with the reformation of the original amine [A]H at the conclusion of the pathway. The presented comparative free energy diagrams (Figure 6) offer significant initial insights into the impact of the amine ligand on the energetics involved in the conversion of CO_2 to methane. Already, we can observe that the presence of the amine ligands tends to stabilize certain types of steps in the reaction process. These findings provide a promising starting point for further investigations and a deeper understanding of the catalytic role of the amine ligand in the CO_2 methanation reaction. First and foremost, the amine ligands promote the adsorption of CO_2 by 0.30 eV (steps 0−2, Figure 6) in the form of carbamic acid. However, the *COOH formation from the carbamic acid and dissociated H_2 is slightly uphill (0.40 eV) in the presence of the amine ligands. The step is thermoneutral otherwise. A kinetic barrier calculation may be necessary for further comparative analysis of the initial adsorption and the reaction of the *COOH species. This species then dissociates into *CO and *OH and the energetics are downhill in both pathways. As pointed out earlier, the amine ligand already stabilizes both the intermediate *COOH and the product species CO*, therefore, the dissociation is less downhill with the assistance of the amine ligands. The exact kinetics of dissociation have not been considered since that is widely covered in the literature.[47−49]

The key differences can also be seen in the subsequent dissociation step CO* ↔ C* + O* (steps 4−6 in the energy diagram, Figure 6). The step is significantly stabilized by the presence of the amine ligand and therefore, the thermodynamics are considerably reversed for the two cases (−0.13 eV in the amine bound vs 0.81 eV in the amine-free pathway). Moreover, as discussed in the respective sections earlier, the amine ligands also lower the barrier by more than 1 eV (Figure 3). Higher stability of CO in the amine-free pathway increases the likelihood of CO poisoning[3] than in the amine-pathway where CO can spontaneously dissociate due to lower barriers. Another considerable difference is in the destabilization of the hydrogenation reaction step C* + H* ↔ CH* (steps 8−11 in the energy diagram, Figure 6). The step may seem less favorable in the presence of the amine (0.48 eV in the amine bound vs −0.18 eV in the amine-free pathway). However, the reaction barrier is similar regardless of the presence of the amine (Figure 4b). As for the second hydrogenation step, the reaction energy is favorably lower in the amine-bound case (Figure 4a). After this step, the amine must unbind from the carbon atom for further hydrogenation to occur. Therefore, the

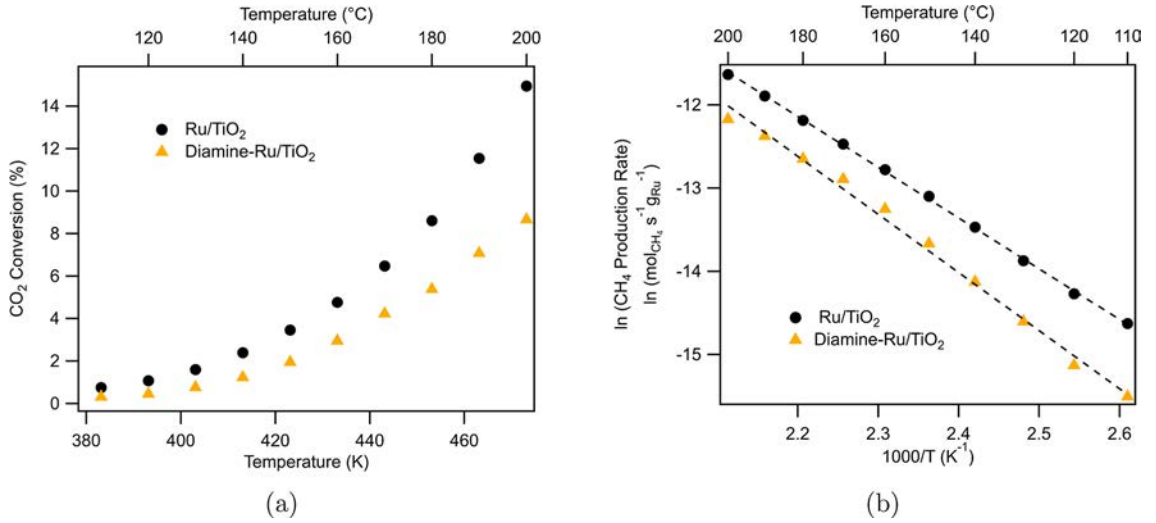


Figure 7. CO_2 conversion (a) and Arrhenius plots (b) for CO_2 methanation over Ru/TiO_2 and diamine-Ru/TiO_2 catalysts in the 110−200 °C temperature range with a 6.67:1 H_2:CO_2 molar ratio.

https://doi.org/10.1021/acs.jpcc.4c08009
J. Phys. Chem. C XXXX, XXX, XXX−XXX

amine-bound and conventional CO_2 methanation pathways can be compared up until this point, after which the pathways share the final two hydrogenation steps from CH_2 to methane. Furthermore, the possibilities of amine ligands unbinding from the carbon at any intermediate stage in the pathway have been discussed in earlier sections (Figure 5). With few exceptions, the pathways are favorably downhill in all cases.

In summary, the comparative free energy diagrams presented in Figure 6 provide a very valuable preliminary overview into the influence of the amine ligand on the energetics of the CO_2 to the methane conversion process. However, microkinetic modeling is necessary for a quantitative analysis of its impact on the overall kinetics as discussed in Section 3.4. Nevertheless, our analysis shows a shift in the likely rate-determining steps: CO dissociation ($CO^* \leftrightarrow C^* + O^*$) and the hydrogenation reaction step ($C^* + H^* \leftrightarrow CH^*$) over the two pathways. This, in itself, is sufficient to paint a qualitative picture for the CO_2 reactive conversion and production to CH_4 assisted by the presence of amine ligands, as shown experimentally (Figure 7b).

3.3. Experimental CO_2 Uptake and Methane Conversion. The experimental CO_2 methanation data over the Ru/TiO_2 and Diamine-Ru/TiO_2 catalysts are displayed in Figure 7b. The Ru/TiO_2 sample exhibited slightly higher conversion at all temperatures than the Diamine-Ru/TiO_2 sample. This could be due to the partial blockage of Ru active sites by the diamine coating.[42] The calculated activation energies for both samples were similar, with 50.7 kJ/mol for Ru/TiO_2 and 58.1 kJ/mol for diamine-Ru/TiO_2. These values are in good agreement with previously reported activation energies for the Sabatier reaction over Ru/TiO_2 catalysts (typically 50−70 kJ/mol).[3,23,57,58] These observations on the product selectivity, CO_2 conversion, and the CH_4 production rates over the two catalysts will be discussed from the theory standpoint in Section 3.4.

3.4. Microkinetic Studies for Comparative Methanation. In the earlier sections, DFT energetics indicated a lower energy pathway (with a lower activation barrier) through the amine-assisted mechanism compared to the conventional (amine-free) pathway. However, experimental results showed a lower conversion and a reduced CH_4 production rate over the diamine-Ru/TiO_2 catalyst compared to the Ru/TiO_2 catalyst. To reconcile this discrepancy, we utilized DFT energetics to propose a microkinetic (MKM) simulation to model the overall CO_2 reactive uptake facilitated by the amine ligands. This simulation includes steps such as amine adsorption, amine−carbon complex (AC) formation and adsorption, CO_2 direct adsorption on Ru surface, methanation reactions, and hydrogen adsorption through both the amine-bound and nonamine-bound routes. The simulation considered only lumped methanation reaction steps M1−M7 (C−O dissociation and C hydrogenation, Table S1) for a quick analysis since these have the highest activation barriers among all the steps. It was assumed that all other intermediate steps were pseudoequilibrated. The adsorbed amines were considered as an inactive species since, as per our DFT analysis (Section 3.1.1), the amine-grafted carbon's reactivity toward methanation is tuned only after the amines form the amine−carbon complex (carbamic acid) and adsorb on the surface. Moreover, the amines easily block surface sites by forming nitrogen-surface bonds, thereby rendering the amine group incapable of CO_2 capture.[34] The readers can refer to Section Supporting Information Note S5 for elaborate details on the MKM, the considered steps, and their energetics.

The MKM simulations were conducted at the experimental reaction and feed operating conditions of $CO_2/He/H_2$ as 1:9:6.67 at 0.85 bar pressure for a range of the reactor temperatures around the experimental values (373−473 K). The initial amine population was represented by an amine concentration corresponding to the experimental grafting concentration of 2.46×10^{-20} moles of amines per Ru nanoparticle (see Supporting Information Note S5, Impact of Amine Coverage on Methanation). The simulations provided data on the coverage of reactants and intermediates at the various temperatures considered, as well as the CH_4 production rates on both the amine-grafted and Ru (amine-free) surfaces. When these production rates are multiplied by the surface coverage of CH_4-producing sites on a Ru nanoparticle, they are converted into turnover frequency (TOF), representing the moles of CH_4 produced per mole of Ru catalyst per unit time. The methodology follows our cross-scale catalyst modeling approach.[59]

The MKM results reveal minimal coverage of the amine−carbon complex ([A]COOH, the reactive species in the amine-bound pathway) and high CO_2 coverage at all reaction temperatures (Figure 8a). Furthermore, the surface predominantly remains covered with dissociated hydrogen (H*) for facilitating hydrogenation, although their coverage decreases with increasing temperature as the adsorbed H desorbs from

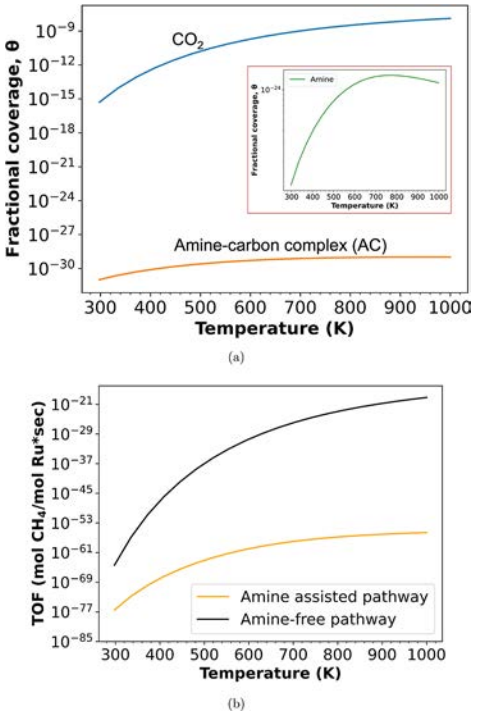


Figure 8. (a) MKM simulated coverage (θ) of adsorbed species—amine ([A]) shown in the inset, amine−CO_2 complex ([A]COOH or AC) and CO_2 on the amine-grafted Ru(0001) surface, and (b) MKM simulated CH_4 production turnover frequency (TOF) via the amine-assisted (amine-bound: orange) and the conventional pathway (nonamine-bound/amine-free:black) toward CO_2 methanation on the Ru(0001) surface. The feed operating conditions are simulated at the experimental feed conditions—$CO_2/He/H_2$ as 1:9:6.67 at the experimental operating pressure of 0.85 bar. The *y*-axis is on a log scale in both plots as well as the inset plot in (a).

https://doi.org/10.1021/acs.jpcc.4c08009
J. Phys. Chem. C XXXX, XXX, XXX−XXX

the surface (S7). Additionally, the surface coverage of amines, modeled as inactive species, remains low across all temperatures and decreases further at higher temperatures.

Though the DFT simulations indicate that amines offer a lower energy pathway (lower C−O dissociation), they are present in lower quantities on the surface to facilitate the conversion. Consequently, less CO_2 follows the amine-bound, lower-energy pathway, while the amine-free CO_2 adsorbed species are more readily available for methanation. This leads to significantly lower CH_4 production via the amine-bound pathway compared to the nonamine pathway (Figure 8b), with the difference becoming more pronounced at higher temperatures as nonamine-bound production surpasses the amine-bound CO_2 conversion. The decreased CO_2 uptake and a decreased conversion on the aminated catalyst also align with our experimental observations (Figure 7b) on CO_2 conversions and the CH_4 production rates, showing only similar methanation rates on nonamine-bound pathways despite being suggested by our theoretical calculations. Interestingly, both the CO_2 conversions and the CH_4 production rates are slightly higher for the nonamine bound case. This can be explained via higher coverage of CO_2 on the surface than the amine−carbon complexes.

Our DFT calculated energetics are also in agreement with the widely reported high selectivity of Ru for CH_4 production[3] and the thermodynamic equilibrium favoring CH_4 over CO at these low reaction temperatures.[4] This can be explained by the significant difference in energetics between the CO binding energy and the subsequent C−O dissociation step toward CH_4 formation in both the amine-bound and the conventional pathways. In the amine-bound case, CO binding energy is −2.39 eV vs −0.13 eV (subsequent C−O dissociation). These values are −4.35 and 0.81 eV, respectively for the conventional pathway. These suggest it is easier energetically (with kinetics considered) for CO to dissociate rather than desorb away from the surface, explaining the high CH_4 selectivity in both pathways, as is commonly observed on Ru.

Finally, the sensitivity of our MKM simulations toward the operating feed conditions for inlet H_2 and CO_2 ratios is detailed in the Supporting Information Note S5. At all feed conditions, the Ru surface is covered with amines, H_2 and CO_2 (Figure S7), suggesting our analysis is not an artifact of the feed initialization conditions. Furthermore, Our MKM analysis shows that while increasing the initial amine concentration (experimental grafting concentration) enhances the amine-assisted methanation TOF, the amine-free pathway consistently exhibits a higher TOF, indicating that the exact amine distribution between the TiO_2 support and Ru is not critical to our conclusions (Supporting Information Note S5, Figure S11). The readers should note that the absolute values for the CH_4 production rates and the adsorbed species coverage are not to be interpreted and compared quantitatively with our experiments since the MKM does not explicitly consider adsorbate−adsorbate interactions and report the rates on per surface site basis. Neither is the exact reaction temperature at which the amine-free pathway surpasses the amine-bound pathway in production rates. The MKM simulations primarily serve to qualitatively bridge the gap between the theoretical DFT simulation-based insights and the experimental findings, which it successfully achieves.

4. CONCLUSIONS

Using DFT calculations with methylamine as a model amine, we proposed a series of elementary reaction steps for the catalytic conversion of amine-bound CO_2 on a Ru(0001) surface, allowing us to identify distinct adsorbed intermediates. The primary goal of our simulations was to determine whether the amine functions mainly as a CO_2 capture agent without significantly impacting catalysis, or if it actively alters the catalytic process. To assess this, we conducted a comparative analysis of the amine-bound and nonamine-bound pathways. Based on DFT energetics, including reaction energies and activation barriers, we found that carbon coordination governs its ability to dissociate and react. The presence of the amine ligand modifies the carbon coordination environment, promoting direct C−O dissociation. Additionally, it appears that amines may destabilize the CO* adsorbate compared to the nonamine-bound case, thereby reducing the risk of CO poisoning-a hypothesis previously suggested. Our results also indicate an energetic preference for hydrogenation, with the relative instability of C* and increased stability of [A]C* making hydrogenation more favorable, although more uphill in the amine-bound scenario. The likelihood of amine unbinding depends on the specific CH_x configuration, with the amine ligand influencing this process.

Despite theoretically predicting a lower energy pathway in the presence of amines, our experiments reported similar CO_2 conversion and CH_4 production rates over both synthesized catalysts "Ru/TiO_2" and the amine (*N*-(2-aminoethyl)-3-aminoproplytrimethoxysilane ("diaminosilane")) deposited catalyst "diamine-Ru/TiO_2". A microkinetic model (MKM) was employed to reconcile these observations with experimental data, suggesting a lower surface coverage of amine−carbon complexes and relatively higher CO_2 coverage at all temperatures to explain this anomaly. Overall, the findings from our DFT calculations provide qualitative insights into the amine-assisted CO_2 uptake, consistent with experimental demonstrations. These results shed light on the mechanisms by which amine ligands, when stabilized on the catalyst surface, play a crucial role in facilitating CO_2 conversion processes. Our DFT calculations offer qualitative insights into the amine-assisted CO_2 uptake, aligning with experimental observations. These findings illuminate how amine ligands, when stabilized on a catalyst surface, play a pivotal role in facilitating CO_2 conversion. The strength of the interaction between amines and the substrate is key to optimizing such processes. By understanding the underlying mechanisms and strategies to enhance this binding, we can better leverage the role of amines. Certain transition metals, such as Fe, and Re, with partially filled d-orbitals, are known to exhibit stronger binding with nitrogen-containing groups.[60] Functionalizing amines with electron-withdrawing groups (like fluorine or chlorine) can decrease the electron density on nitrogen, making it more electrophilic and improving its binding affinity to electron-rich metal surfaces, such as Pt.[21,61] However, the binding strength should be balanced to avoid oversaturating the metal surface, ensuring that key catalytic sites, like those required for H_2 dissociation in methanation, remain accessible for optimal catalytic activity.

https://doi.org/10.1021/acs.jpcc.4c08009
J. Phys. Chem. C XXXX, XXX, XXX−XXX

■ ASSOCIATED CONTENT

Supporting Information

The Supporting Information is available free of charge at https://pubs.acs.org/doi/10.1021/acs.jpcc.4c08009.

A description of the amine model construction; Ru(0001) slab model; aminosilane grafting on Ru/TiO_2: distribution and potential interactions with metal sites; established energetics for conversion of captured CO_2 into CH_4 and microkinetics for conversion of captured CO_2 into CH_4 (PDF)

■ AUTHOR INFORMATION

Corresponding Authors

Shyam Deo − *Materials Science Division, Lawrence Livermore National Laboratory, Livermore, California 94550, United States; Laboratory for Energy Applications of the Future, Lawrence Livermore National Laboratory, Livermore, California 94550, United States;* orcid.org/0000-0002-3590-4398; Email: deo4@llnl.gov

Sneha A. Akhade − *Materials Science Division, Lawrence Livermore National Laboratory, Livermore, California 94550, United States; Laboratory for Energy Applications of the Future, Lawrence Livermore National Laboratory, Livermore, California 94550, United States;* orcid.org/0000-0003-0024-2299; Email: akhade1@llnl.gov

Authors

Thomas Ludwig − *Materials Science Division, Lawrence Livermore National Laboratory, Livermore, California 94550, United States*

Melinda L. Jue − *Materials Science Division, Lawrence Livermore National Laboratory, Livermore, California 94550, United States; Laboratory for Energy Applications of the Future, Lawrence Livermore National Laboratory, Livermore, California 94550, United States;* orcid.org/0000-0002-6864-2419

Nathan C. Ellebracht − *Materials Science Division, Lawrence Livermore National Laboratory, Livermore, California 94550, United States; Laboratory for Energy Applications of the Future, Lawrence Livermore National Laboratory, Livermore, California 94550, United States;* orcid.org/0000-0001-6815-4936

Mathew J. Rasmussen − *National Bioenergy Center, National Renewable Energy Laboratory, Golden, Colorado 80401, United States*

James M. Crawford − *Department of Chemical & Biological Engineering, Montana State University, Bozeman, Montana 59717, United States;* orcid.org/0000-0003-3614-6055

Matthew M. Yung − *National Bioenergy Center, National Renewable Energy Laboratory, Golden, Colorado 80401, United States*

Simon H. Pang − *Materials Science Division, Lawrence Livermore National Laboratory, Livermore, California 94550, United States; Laboratory for Energy Applications of the Future, Lawrence Livermore National Laboratory, Livermore, California 94550, United States;* orcid.org/0000-0003-2913-1648

Complete contact information is available at: https://pubs.acs.org/10.1021/acs.jpcc.4c08009

Author Contributions

[⊥]S.D. and T.L. contributed equally to this work.

Notes

The authors declare no competing financial interest.

■ ACKNOWLEDGMENTS

This work was supported by the U.S. Department of Energy Office of Fossil Energy and Carbon Management under grant FWP-FEW0277. This work was performed under the auspices of the U.S. Department of Energy by the Lawrence Livermore National Laboratory under contract DE-AC52-07NA27344. LLNL release number: LLNL-JRNL-870158.

■ REFERENCES

(1) Shen, X.; Du, H.; Mullins, R. H.; Kommalapati, R. R. Polyethylenimine Applications in Carbon Dioxide Capture and Separation: From Theoretical Study to Experimental Work. *Energy Technol.* **2017**, *5*, 822−833.

(2) Choi, S.; Drese, J. H.; Jones, C. W. Adsorbent materials for carbon dioxide capture from large anthropogenic point sources. *ChemSusChem* **2009**, *2*, 796−854.

(3) Panagiotopoulou, P. Hydrogenation of CO2 over supported noble metal catalysts. *Appl. Catal., A* **2017**, *542*, 63−70.

(4) Lee, W. J.; Li, C.; Prajitno, H.; Yoo, J.; Patel, J.; Yang, Y.; Lim, S. Recent trend in thermal catalytic low temperature CO2 methanation: A critical review. *Catal. Today* **2021**, *368*, 2−19.

(5) Müller, K.; Fleige, M.; Rachow, F.; Schmeißer, D. Sabatier based CO2-methanation of Flue Gas Emitted by Conventional Power Plants. *Energy Procedia* **2013**, *40*, 240−248.

(6) Türks, D.; Mena, H.; Armbruster, U.; Martin, A. Methanation of CO2 on Ni/Al2O3 in a Structured Fixed-Bed Reactor—A Scale-Up Study. *Catalysts* **2017**, *7*, 152.

(7) Frontera, P.; Macario, A.; Ferraro, M.; Antonucci, P. Supported Catalysts for CO2Methanation: A Review. *Catalysts* **2017**, *7*, 59.

(8) Stangeland, K.; Kalai, D.; Li, H.; Yu, Z. CO2Methanation: The Effect of Catalysts and Reaction Conditions. *Energy Procedia* **2017**, *105*, 2022−2027.

(9) Kothandaraman, J.; Dagle, R. A.; Dagle, V. L.; Davidson, S. D.; Walter, E. D.; Burton, S. D.; Hoyt, D. W.; Heldebrant, D. J. Condensed-phase low temperature heterogeneous hydrogenation of CO2 to methanol. *Catal. Sci. Technol.* **2018**, *8*, 5098−5103.

(10) Duyar, M. S.; Wang, S.; Arellano-Treviño, M. A.; Farrauto, R. J. CO2 utilization with a novel dual function material (DFM) for capture and catalytic conversion to synthetic natural gas: An update. *J. CO_2 Util.* **2016**, *15*, 65−71.

(11) Tian, S.; Yan, F.; Zhang, Z.; Jiang, J. Calcium-looping reforming of methane realizes in situ CO2 utilization with improved energy efficiency. *Sci. Adv.* **2019**, *5*, No. eaav5077.

(12) Shao, B.; Hu, G.; Alkebsi, K. A. M.; Ye, G.; Lin, X.; Du, W.; Hu, J.; Wang, M.; Liu, H.; Qian, F. Heterojunction-redox catalysts of FexCoyMg10CaO for high-temperature CO2 capture and in situ conversion in the context of green manufacturing. *Energy Environ. Sci.* **2021**, *14*, 2291−2301.

(13) Siegel, R. E.; Pattanayak, S.; Berben, L. A. Reactive Capture of CO2: Opportunities and Challenges. *ACS Catal.* **2023**, *13*, 766−784.

(14) Zhang, Y.; Zhao, S.; Li, L.; Feng, J.; Li, K.; Huang, Z.; Lin, H. Integrated CO2 capture and utilization: a review of the synergistic effects of dual function materials. *Catal. Sci. Technol.* **2024**, *14*, 790−819.

(15) Olah, G. A.; Prakash, G. K. S.; Goeppert, A. Anthropogenic Chemical Carbon Cycle for a Sustainable Future. *J. Am. Chem. Soc.* **2011**, *133*, 12881−12898.

(16) Wang, S.; Schrunk, E. T.; Mahajan, H.; Farrauto, A. R. J. The Role of Ruthenium in CO2 Capture and Catalytic Conversion to Fuel by Dual Function Materials (DFM). *Catalysts* **2017**, *7*, 88.

(17) Duyar, M. S.; Treviño, M. A. A.; Farrauto, R. J. Dual function materials for CO2 capture and conversion using renewable H2. *Appl. Catal., B* **2015**, *168*−*169*, 370−376.

(18) Sun, H.; Wang, J.; Zhao, J.; Shen, B.; Shi, J.; Huang, J.; Wu, C. Dual functional catalytic materials of Ni over Ce-modified CaO

sorbents for integrated CO2 capture and conversion. *Appl. Catal., B* **2019**, *244*, 63−75.
(19) Arellano-Treviño, M. A.; Kanani, N.; Jeong-Potter, C. W.; Farrauto, R. J. Bimetallic catalysts for CO2 capture and hydrogenation at simulated flue gas conditions. *Chem. Eng. J.* **2019**, *375*, 121953.
(20) Li, S.; Cerón, M. R.; Eshelman, H. V.; Varni, A. J.; Maiti, A.; Akhade, S.; Pang, S. H. Probing the Kinetic Origin of Varying Oxidative Stability of Ethyl- vs. Propyl-spaced Amines for Direct Air Capture. *ChemSusChem* **2023**, *16*, No. e202201908.
(21) Zhang, J.; Deo, S.; Janik, M. J.; Medlin, J. W. Control of Molecular Bonding Strength on Metal Catalysts with Organic Monolayers for CO2 Reduction. *J. Am. Chem. Soc.* **2020**, *142*, 5184−5193.
(22) Yu, J.; Zeng, Y.; Jin, Q.; Lin, W.; Lu, X. Hydrogenation of CO2 to Methane over a Ru/RuTiO2 Surface: A DFT Investigation into the Significant Role of the RuO2 Overlayer. *ACS Catal.* **2022**, *12*, 14654−14666.
(23) Crawford, J. M.; Petel, B. E.; Rasmussen, M. J.; Ludwig, T.; Miller, E. M.; Halingstad, S.; Akhade, S. A.; Pang, S. H.; Yung, M. M. Influence of residual chlorine on Ru/TiO2 active sites during CO2 methanation. *Appl. Catal., A* **2023**, *663*, 119292.
(24) Akamaru, S.; Shimazaki, T.; Kubo, M.; Abe, T. Density functional theory analysis of methanation reaction of CO2 on Ru nanoparticle supported on TiO2 (1 0 1). *Appl. Catal., A* **2014**, *470*, 405−411.
(25) Hohenberg, P.; Kohn, W. Inhomogeneous Electron Gas. *Phys. Rev.* **1964**, *136*, B864−B871.
(26) Kresse, G.; Hafner, J. Ab initio molecular dynamics for liquid metals. *Phys. Rev. B* **1993**, *47*, 558−561.
(27) Kresse, G.; Furthmüller, J. Efficiency of ab-initio total energy calculations for metals and semiconductors using a plane-wave basis set. *Comput. Mater. Sci.* **1996**, *6*, 15−50.
(28) Kresse, G.; Furthmüller, J. Efficient iterative schemes for ab initio total-energy calculations using a plane-wave basis set. *Phys. Rev. B* **1996**, *54*, 11169−11186.
(29) Larsen, A. H.; Mortensen, J. J.; Blomqvist, J.; Castelli, I. E.; Christensen, R.; Dułak, M.; Friis, J.; Groves, M. N.; Hammer, B.; Hargus, C.; et al. The atomic simulation environment—a Python library for working with atoms. *J. Phys.: Condens. Matter* **2017**, *29*, 273002.
(30) Hammer, B.; Hansen, L. B.; Nørskov, J. K. Improved adsorption energetics within density-functional theory using revised Perdew-Burke-Ernzerhof functionals. *Phys. Rev. B* **1999**, *59*, 7413−7421.
(31) Blöchl, P. E. Projector augmented-wave method. *Phys. Rev. B* **1994**, *50*, 17953−17979.
(32) Kresse, G.; Joubert, D. From ultrasoft pseudopotentials to the projector augmented-wave method. *Phys. Rev. B* **1999**, *59*, 1758−1775.
(33) Methfessel, M.; Paxton, A. High-precision sampling for Brillouin-zone integration in metals. *Phys. Rev. B* **1989**, *40*, 3616.
(34) Müller, K.; Lu, D.; Senanayake, S. D.; Starr, D. E. Monoethanolamine Adsorption on TiO2(110): Bonding, Structure, and Implications for Use as a Model Solid-Supported CO2 Capture Material. *J. Phys. Chem. C* **2014**, *118*, 1576−1586.
(35) Lee, A. S.; Kitchin, J. R. Chemical and Molecular Descriptors for the Reactivity of Amines with CO2. *Ind. Eng. Chem. Res.* **2012**, *51*, 13609−13618.
(36) Yoo, C.-J.; Lee, L.-C.; Jones, C. W. Probing Intramolecular versus Intermolecular CO2 Adsorption on Amine-Grafted SBA-15. *Langmuir* **2015**, *31*, 13350−13360.
(37) Sharma, P.; Chakrabarty, S.; Roy, S.; Kumar, R. Molecular View of CO2 Capture by Polyethylenimine: Role of Structural and Dynamical Heterogeneity. *Langmuir* **2018**, *34*, 5138−5148.
(38) Kim, K. C.; Moschetta, E. G.; Jones, C. W.; Jang, S. S. Molecular Dynamics Simulations of Aldol Condensation Catalyzed by Alkylamine-Functionalized Crystalline Silica Surfaces. *J. Am. Chem. Soc.* **2016**, *138*, 7664−7672.
(39) Mohan, O.; Shambhawi, S.; Xu, R.; Lapkin, A. A.; Mushrif, S. H. Investigating CO_2 Methanation on Ni and Ru: DFT Assisted Microkinetic Analysis. *ChemCatChem* **2021**, *13*, 2420−2433.
(40) Bengtsson, L. Dipole correction for surface supercell calculations. *Phys. Rev. B* **1999**, *59*, 12301−12304.
(41) Henkelman, G.; Uberuaga, B. P.; Jónsson, H. A climbing image nudged elastic band method for finding saddle points and minimum energy paths. *J. Chem. Phys.* **2000**, *113*, 9901−9904.
(42) McNeary, W. W.; Ellebracht, N. C.; Jue, M. L.; Rasmussen, M. J.; Crawford, J. M.; Yung, M. M.; To, A. T.; Pang, S. H. Application of Solid-Supported Amines for Thermocatalytic Reactive CO2 Capture. *ACS Omega* **2025**, *10*, 2364−2371.
(43) Yang, J.; Pell, A. J.; Hedin, N.; Lyubartsev, A. Computational insight into the hydrogenation of CO2 and carbamic acids to methanol by a ruthenium(II)-based catalyst: The role of amino (NH) ligand group. *Mol. Catal.* **2021**, *506*, 111544.
(44) Szego, A. E.; Church, T. L.; Bacsik, Z.; Jaworski, A.; Ullah, L.; Hedin, N. Precapture of CO2 and Hydrogenation into Methanol on Heterogenized Ruthenium and Amine-Rich Catalytic Systems. *ChemistryOpen* **2023**, *12*, No. e202300060.
(45) Zhou, Y.; Zhao, Y.; Shi, X.; Tang, Y.; Yang, Z.; Pu, M.; Lei, M. A theoretical study on the hydrogenation of CO2 to methanol catalyzed by ruthenium pincer complexes. *Dalton Trans.* **2022**, *51*, 10020−10028.
(46) Versteeg, G.; van Swaaij, W. On the kinetics between CO2 and alkanolamines both in aqueous and non-aqueous solutions—I. Primary and secondary amines. *Chem. Eng. Sci.* **1988**, *43*, 573−585.
(47) Sahebdelfar, S.; Takht Ravanchi, M. Carbon dioxide utilization for methane production: A thermodynamic analysis. *J. Pet. Sci. Eng.* **2015**, *134*, 14−22.
(48) Wang, X.; Hong, Y.; Shi, H.; Szanyi, J. Kinetic modeling and transient DRIFTS-MS studies of CO2 methanation over Ru/Al2O3 catalysts. *J. Catal.* **2016**, *343*, 185−195.
(49) Avanesian, T.; Gusmão, G. S.; Christopher, P. Mechanism of CO2 reduction by H2 on Ru(0 0 0 1) and general selectivity descriptors for late-transition metal catalysts. *J. Catal.* **2016**, *343*, 86−96.
(50) Calegari Andrade, M. F.; Li, S.; Pham, T. A.; Akhade, S. A.; Pang, H. Machine learning demonstrates the impact of proton transfer and solvent dynamics on CO_2 capture in liquid ammonia. *Chem. Sci.* **2024**, *15*, 13173−13180.
(51) Chen, W.; Cao, J.; Fu, W.; Zhang, J.; Qian, G.; Yang, J.; Chen, D.; Zhou, X.; Yuan, W.; Duan, X. Molecular-Level Insights into the Notorious CO Poisoning of Platinum Catalyst. *Angew. Chem., Int. Ed.* **2022**, *61*, No. e202200190.
(52) Wang, J.; Kawazoe, Y.; Sun, Q.; Chan, S.; Su, H. The selectivity and activity of catalyst for CO hydrogenation to methanol and hydrocarbon: A comparative study on Cu, Co and Ni surfaces. *Surf. Sci.* **2016**, *645*, 30−40.
(53) Krösschell, R. D.; Hensen, E. J.; Filot, I. A. Unravelling CO Activation on Flat and Stepped Co Surfaces: A Molecular Orbital Analysis. *J. Phys. Chem. C* **2024**, *128*, 8947−8960.
(54) Zhang, H.; Goeppert, A.; Olah, G. A.; Prakash, G. K. S. Remarkable effect of moisture on the CO2 adsorption of nano-silica supported linear and branched polyethylenimine. *J. CO_2 Util.* **2017**, *19*, 91−99.
(55) Veneman, R.; Frigka, N.; Zhao, W.; Li, Z.; Kersten, S.; Brilman, W. Adsorption of H2O and CO2 on supported amine sorbents. *Int. J. Greenhouse Gas Control* **2015**, *41*, 268−275.
(56) Solis-Garcia, A.; Louvier-Hernandez, J. F.; Almendarez-Camarillo, A.; Fierro-Gonzalez, J. C. Participation of surface bicarbonate, formate and methoxy species in the carbon dioxide methanation catalyzed by ZrO2-supported Ni. *Appl. Catal., B* **2017**, *218*, 611−620.
(57) Kim, A.; Debecker, D. P.; Devred, F.; Dubois, V.; Sanchez, C.; Sassoye, C. CO2 methanation on Ru/TiO2 catalysts: On the effect of mixing anatase and rutile TiO2 supports. *Appl. Catal., B* **2018**, *220*, 615−625.

https://doi.org/10.1021/acs.jpcc.4c08009
J. Phys. Chem. C XXXX, XXX, XXX−XXX

(58) Petala, A.; Panagiotopoulou, P. Methanation of CO2 over alkali-promoted Ru/TiO2 catalysts: I. Effect of alkali additives on catalytic activity and selectivity. *Appl. Catal., B* **2018**, *224*, 919−927.
(59) Deo, S.; Sun, W.; Chatterjee, T.; Moore, T.; Yuan, M.; Mcnenly, M. J.; Akhade, S. A.; Bucci, G. Cross-Scale Catalyst Modeling Applied to H2 Storage and Release via Formic Acid. *Ind. Eng. Chem. Res.* **2025**, *64*, 1439−1448.
(60) Vojvodic, A.; Nørskov, J. K. New design paradigm for heterogeneous catalysts. *Natl. Sci. Rev.* **2015**, *2*, 140−143.
(61) Jiang, Y.-F.; Liu, J.-C.; Xu, C.-Q.; Li, J.; Xiao, H. Breaking the scaling relations for efficient N2-to-NH3 conversion by a bowl active site design: Insight from LaRuSi and isostructural electrides. *Chin. J. Catal.* **2022**, *43*, 2183−2192.

https://doi.org/10.1021/acs.jpcc.4c08009
J. Phys. Chem. C XXXX, XXX, XXX−XXX